

The low-power nucleus of PKS 1246–410 in the Centaurus Cluster

G. B. Taylor^{1,2,3}, J. S. Sanders⁴, A. C. Fabian⁴, and S. W. Allen¹

ABSTRACT

We present Chandra, Very Large Array (VLA), and Very Long Baseline Array (VLBA) observations of the nucleus of NGC 4696, a giant elliptical in the Centaurus cluster of galaxies. Like M87 in the Virgo cluster, PKS 1246–410 in the Centaurus cluster is a nearby example of a radio galaxy in a dense cluster environment. In analyzing the new X-ray data we have found a compact X-ray feature coincident with the optical and radio core. While nuclear emission from the X-ray source is expected, its luminosity is low, $< 10^{40}$ erg s⁻¹. We estimate the Bondi accretion radius to be 30 pc and the accretion rate to be 0.01 M_⊙ y⁻¹ which under the canonical radiative efficiency of 10% would overproduce by 3.5 orders of magnitude the radiative luminosity. Much of this energy can be directed into the kinetic energy of the jet, which over time inflates the observed cavities seen in the thermal gas. The VLBA observations reveal a weak nucleus and a broad, one-sided jet extending over 25 parsecs in position angle -150 degrees. This jet is deflected on the kpc-scale to a more east-west orientation (position angle of -80 degrees).

Subject headings: galaxies: clusters: individual (Centaurus) – intergalactic medium – accretion – radio continuum: galaxies

¹Kavli Institute of Particle Astrophysics and Cosmology, Stanford University, Stanford, CA 94305, USA; swa@stanford.edu

²National Radio Astronomy Observatory, Socorro, NM 87801, USA

³University of New Mexico, Dept. of Physics and Astronomy, Albuquerque, NM 87131, USA; gbtaylor@unm.edu

⁴Institute of Astronomy, Madingley Road, Cambridge CB3 0HA, UK; jss, acf@ast.cam.ac.uk

1. Introduction

The Centaurus cluster, Abell 3526, is a nearby (redshift $z=0.0104$), X-ray bright galaxy cluster. At the center of this cluster is the bright elliptical galaxy NGC 4696, hosting a moderately powerful radio source, PKS 1246–410. We have been engaged in detailed studies of the X-ray and radio emission from this cluster (Sanders & Fabian 2002; Taylor et al. 2002), and have recently obtained a further 200 ksec of Chandra data (Fabian et al. 2005). Our new Chandra image (Fig. 1), reveals a complex structure within the central few kiloparsecs. A plume-like structure swirls clockwise to the NE and wraps around the radio source. There are clear signs of interaction between the X-ray and radio emission including: (1) strong X-ray emission that matches the shape of the radio emission just south of the core; (2) a faint rim of hard X-ray emission along the northern edge of the radio source; and (3) deep cavities in the X-ray emission on both the east and west sides. We also find a compact X-ray component coincident with the radio and optical core (see Fig. 2).

In order to gain insights to the nature of the nucleus, we have conducted a short, 3 hour, Very Long Baseline Array (VLBA) observation of PKS 1246–410 at 5 GHz. We also present a radio continuum spectrum of the nucleus using the Very Large Array (VLA). Both the VLA and VLBA are operated by the NRAO¹.

Throughout this paper we assume $H_0 = 70 \text{ km s}^{-1} \text{ Mpc}^{-1}$ so that $1'' = 210 \text{ pc}$ at the redshift of the Centaurus cluster.

2. VLA Observations

VLA observations of the radio source PKS 1246–410 were made on 2004 October 24 at 0.326, 1.400, 4.860, 8.460, 14.940, 22.460, and 43.3140 GHz in the “A” configuration. We also make use of previous VLA observations at 4.8 and 8.3 GHz described in Taylor et al. (2002). Details regarding all radio observations are given in Table 1. The source 3C 286 was used as the primary flux density calibrator. Phase calibration was derived from the nearby compact source J1316–3338 except for the observations at 0.326 GHz which employed a more distant, but stronger calibrator at this frequency, J1154-3505. These 0.326 GHz observations have been described by Fabian et al. (2005). Due to poor atmospheric weather conditions at the VLA on 2004 October 24, phase transfer failed for the observations at 43 GHz. At this high frequency, PKS 1246–410 is too weak to self-calibrate and we were only able to obtain an

¹The National Radio Astronomy Observatory is operated by Associated Universities, Inc., under cooperative agreement with the National Science Foundation.

upper limit of 37 mJy on the flux density of the nucleus.

The data were reduced in AIPS (Astronomical Image Processing System) following the standard procedures, and imaged with Difmap. In Fig. 3 we show a spectrum of the nucleus on 2004 Oct 24. These data are tabulated in Table 2. The resolution is proportional to frequency and varies from $\sim 0.07''$ at 43 GHz to $\sim 10''$ at 0.32 GHz. Consequently, some lobe emission contaminates the spectrum of the nucleus at 1.4 GHz, and we cannot estimate the nuclear flux density at 0.32 GHz. We find a powerlaw with slope, $\alpha = -0.55 \pm 0.04$ describes the nuclear spectrum well between 1.4 and 43 GHz. We define the spectral index, α , as $S_\nu \propto \nu^\alpha$.

3. VLBA Observations

The VLBA observed PKS 1246–410 at 5.0 GHz on 2005 February 14, with only 9 antennas since the VLBA station at Brewster, WA, is too far north to observe this southern source. A total of 32 MHz bandwidth was recorded in both right and left circular polarization using 2 bit sampling. The nearby (1.0°) source J1253-4059 was used for phase-referencing with a 1:1 minute cycle on source:calibrator. The more distant (5.1°) calibrator J1227-4436 was observed every 30 minutes to check on the quality of the phase referencing and gain calibration. Unfortunately, this source was so distant that the phase-referencing did not succeed. The total time on PKS 1246–410 was 66 minutes.

Amplitude calibration was derived using measurements of the system temperatures and antenna gains at 4992 MHz. Fringe-fitting was performed with the AIPS task FRING on the strong calibrator 3C 279. Before the final application of the fringe-calibration, PKS 1246–410 was shifted by 136 mas west, and 308 mas south based on a preliminary measurement of its position from these observations. The best position of the nucleus, along with other radio properties, is summarized in Table 3. Bandpass calibration was derived from the observation of 3C 279. No linear polarization calibration was attempted for this short observing run. Self-calibration with a 1 minute solution interval was used to further refine the calibration and remove some slow-changing atmospheric phase errors.

The final image at full resolution (Fig.4) has an rms noise of $90 \mu\text{Jy}/\text{beam}$. The full resolution VLBA image reveals a compact component with 9 mJy, and a bright inner jet of flux density 2.4 mJy at position angle -156° . A tapered image (Fig. 5) shows that the jet is broad (opening angle 18°) and can be traced out over 120 mas in position angle -152° . The total flux density recovered in the VLBA image is 29 mJy. This is 31% of the 94.4 mJy seen in the central $0.4''$ by the VLA, suggesting that two thirds of the flux exists on intermediate

(50 pc) scales. The nearly north-south alignment of the parsec-scale jet agrees well with the initial orientation suggested by high resolution VLA images (e.g., Fig. 1). These radio properties are similar to those of other nearby low power radio galaxies (Giovannini et al. 2005).

4. Chandra Observations

The data presented here are from five Chandra observations listed in Table 7. Each of these observations were taken using the ACIS-S3 back-illuminated CCD. The level 1 event files were reprocessed by CIAO 3.2 using gain file `acisD2000-01-29gain_ctiN0003.fits`. The count rate in the 2.5 to 7 keV band on ACIS-S1 was used to filter out periods with flares using the CIAO `LC_CLEAN` tool, yielding a total exposure time of 196.6 ks for the X-ray images presented here. Each of the observations were reprojected to have the same coordinate system as observation 4954.

For spectral analysis, we extracted spectra for a particular region from each of the event files. Response matrices and ancillary response matrices for each spectrum were created using the `MKACISRMF` and `MKWARF` tools. Background spectra were extracted from the same spatial regions on the chip. These background event files were created from blank sky observations, reprocessed and reprojected to have the same coordinate system. Source spectra from each run were added together to form a total spectrum. A total weighted response and ancillary response was created by adding together the individual responses, weighting according to the number of counts in the 0.5 to 7 keV band of their respective foreground spectrum. The background spectra were added, with the appropriate weight.

Chandra X-ray observations of the central region (Fig. 2) reveal a compact source coincident with the compact radio core of PKS 1246–410. Registration between the X-ray and radio images was tested using observations of a serendipitous background AGN located 2 arcminutes east of PKS 1246–410. At 5 GHz a 19 mJy source is detected at RA (J2000) $12\ 49\ 06.250 \pm 0.01$ and Declination (J2000) $-41\ 17\ 50.414 \pm 0.1$. The source is radially smeared due to the large distance from the center and wide bandwidth used. The source is also detected in the X-rays at RA (J2000) $12\ 49\ 06.231 \pm 0.05$ and Declination (J2000) $-41\ 17\ 50.086 \pm 0.6$. The good agreement between the X-ray and radio positions (Fig. 2) indicates that the Chandra observations were at least as good as its nominal astrometry of 0.6 arcseconds (Aldcroft et al. 2000). This astrometry also results in good agreement with the location of the optical nucleus (see Fig. 6). Hubble Space Telescope (HST) observations by Laine et al. (2003) reveal a double optical nucleus with separation ~ 0.25 arcseconds oriented along a position angle of ~ -120 with the brighter component to the south-east. The

optical astrometry, however, is not sufficiently accurate to identify which optical component is coincident with the subparsec-scale radio core shown in Fig. 4.

The X-ray emission from the location of the nucleus was extracted within a circle centred on 12 48 49.26, $-41\ 18\ 39.52$ (J2000), of radius 0.95 arcsec. The background region was a sector centred on the same position, between radii of 1.11 and 2.67 arcsec, and at an angle of between 6.9 and 215.9° measured from north towards the east. This region excludes the bright thermal emission to the north and west of the nucleus. While compact, we cannot estimate a size for the nucleus more precise than ~ 0.5 arcseconds owing to the bright and complex emission in the central region. In Fig. 7 we show a fit to the central source using a mekal spectrum, with the absorption taken from the Dickey & Lockman (1990) results. Although an additional free absorption component at the redshift of the cluster was allowed, the best fit result required no additional absorption. The best fitting parameters are a temperature of 0.75 ± 0.06 keV, and an abundance of 0.22 ± 0.03 solar (Anders & Grevesse 1989). A power-law model did not provide a good fit to the data. The temperature distribution in the central region of the cluster derived from the X-ray observations is shown in Fig. 8. To create the temperature and absorption maps, spatial regions in the X-ray image containing approximately 400 counts between 0.5 and 7 keV were chosen using the bin accretion tessellation algorithm of Cappellari & Copin (2003). Spectra from these region were independently fit using a mekal model with free absorption, temperature, abundance and normalization in the same energy range using C-statistics. The resulting temperature and absorption maps were smoothed with a Gaussian of 0.49 arcseconds for display purposes. The statistical uncertainty on the temperature is around 0.05 keV in the central regions, and the absorption is uncertain by about $0.05 \times 10^{22} \text{ cm}^{-2}$.

To refine our estimate of the central density we fit a two-temperature mekal model in several incomplete annuli (see Fig. 9). The regions were chosen to avoid contamination from the bright thermal emission to the east, and from the plume. In this way we attempt to calculate the undisturbed density profile in the central region of the Centaurus cluster (Fig. 10). By fitting a two-temperature model this includes the effect of hotter gas projected on top of colder gas at the center of the cluster, or any other multiphase material. Fitting a model in which the density varies as a power law function of the radius to all but the central point (which could be contaminated by nuclear emission) we find an electron density:

$$n_e = (0.082 \pm 0.03)(r)^{-0.46 \pm 0.15} \text{cm}^{-3}$$

where r is given in arcseconds.

No significant change in temperature or abundance is present at the location of the nucleus. The luminosity of the thermal component is 3.7×10^{39} erg/s between 0.1 and 10 keV. Using a powerlaw index of 1.7, and allowing for absorption on the nucleus in addition

to that on the thermal component, we derive a 3-sigma upper limit of 1.2×10^{40} erg/s in the 2-10 keV band for any non-thermal power-law component (corrected for absorption).

5. The Jet of PKS 1246–410

No counterjet is in evidence on parsec-scales, suggesting that the nucleus is Doppler boosted. The 3σ limit on the counterjet side is 0.27 mJy, providing a minimum jet:counterjet ratio of 9:1 for the inner jet. For the jet component at 115 mas, the surface brightness reaches 2.7 mJy/beam in the tapered image, and a counterjet could be detected as faint as 0.45 mJy/beam, so the lower limit on the jet:counterjet ratio is 6:1. Significant Doppler boosting would produce a counterjet component closer to the nucleus, and more compact so it is this counterpart to the larger component that we would more naturally detect. Assuming a spectral index of $\nu^{-0.5}$, we find $\beta\cos(\theta) > 0.34$, implying an orientation of less than 70° from the line-of-sight and a minimum jet velocity of 0.3 c (Lorentz factor, $\gamma > 1.05$). This may indicate that projection effects are also important on larger scales for the radio emission, although there is some evidence that the orientation of the jet is strongly modified on kiloparsec scales. It could be that dense thermal material has stopped the expansion of the source in the north-south direction, and that deceleration of the jet occurs on small scales in cooling core clusters as seen in other cooling core sources previously studied with VLBI (e.g., Hydra A, Taylor 1996 ; A2597, Taylor et al. 1999).

Another estimate of the Lorentz factor of the jet can be obtained from assuming a freely expanding jet (e.g., Salvati et al. 1998) which is expected to show an intrinsic opening angle of $1/\gamma$. Under this assumption we estimate from the observed opening angle of 18° a Lorentz factor of 3.2. This could be less due to projection effects if the jet is pointed close to the line-of-sight. A consistent solution can be obtained with $\gamma = 3.2$, $\beta = 0.95$, and an orientation of 69° from the line-of-sight (i.e., fairly close to the plane of the sky).

We can estimate the minimum kinetic energy of the jet from the energy required to evacuate the bubbles in the two lobes. These energies are 4.5×10^{55} erg for the eastern bubble, and 3.7×10^{55} erg for the western bubble (Dunn & Fabian 2004). Assuming an age for the bubbles of 3×10^6 years (corresponding to an average growth rate of 0.03 c from buoyancy arguments by Dunn & Fabian), we get a mechanical energy input required from the jets of 8×10^{41} erg s^{-1} . With a factor of 4 ($\gamma/(\gamma - 1)$ with $\gamma = 4/3$) for the total energy in relativistic particles in a bubble, together with a factor for the lobes being overpressured since they are growing, the output could be up to ten times larger. This falls about a factor 3 short of the X-ray cooling luminosity, required to stem a cooling catastrophe in a few Gyr, or about 2×10^{43} erg s^{-1} .

6. The Central Engine of PKS 1246–410

In either case of an active galactic nucleus (AGN) seen directly, or indirectly via heating, the nucleus has a relatively low power compared to radio galaxies of similar radio luminosity (Di Matteo et al. 2000; Reich et al. 2000; Donato et al. 2004). Absorption does not seem to be important, so the accretion onto the core must be radiatively inefficient. The large inclination angle of $\sim 70^\circ$ (see §5) is consistent with the relation between core X-ray power and inclination angle found by Donato et al. (2004) for a sample of FR I radio galaxies. Donato et al. (2004) suggest that the decreasing X-ray luminosity with increasing inclination is caused by beaming of the X-ray emission. This can be explained if a substantial fraction of the non-thermal X-ray emission is produced by the Doppler-boosted jet.

Bernardi et al. (2002) measure a velocity dispersion, σ , in NGC 4696 of 262 km s^{-1} . Using the $M_{BH} - \sigma$ relation derived by Pinkney et al. (2003) for 10 early-type galaxies, this velocity dispersion translates to a black hole mass, M_{BH} , of $3 \times 10^8 M_\odot$ with an uncertainty of about a factor of 2. This is close to that estimated by Fujita & Reiprich (2004), based on the same measurements of σ by Bernardi et al. (2002) and the $M_{BH} - \sigma$ relation derived by Gebhardt et al. (2000).

The Bondi accretion radius, r_A , where the gravitational potential dominates over the thermal energy, for a black hole of mass M_{BH} is given by

$$r_A = GM_{BH}m_p/kT$$

where m_p is the proton mass, and T is the temperature of the accreting material. From this we derive a Bondi accretion radius of 30 pc. At the distance of PKS 1246–410 this corresponds to a radius of 0.14 arcsec, which is not resolved by our X-ray observations. From our fit to the density profile from §4, at 0.14 arcsec we estimate an electron density of 0.2 cm^{-3} with an uncertainty of a factor of 2. The Bondi accretion rate within this radius is

$$\dot{M} = 4\pi r_A^2 \rho c_s$$

where ρ is the density, and c_s is the sound speed given by $c_s \sim 2.7 \times 10^7 T_{0.8}^{1/2} \text{ cm s}^{-1}$ with $T_{0.8} = T/0.8 \text{ keV}$ the ISM temperature in units of keV. For PKS 1246–410 we find an accretion rate of $0.014 M_\odot \text{ y}^{-1}$. Assuming a 10% conversion efficiency into radiation, this predicts a luminosity of $8 \times 10^{43} \text{ erg s}^{-1}$. This luminosity is nearly four orders of magnitude more than observed in X-rays (§4), or to put it another way, the radiative efficiency, η , is $\sim 2 \times 10^{-4}$. We can also compare the accretion energy output to that of the jet (§5), and find that it is an order of magnitude larger than required to blow the bubbles. It could be that the Bondi accretion has been suppressed somewhat by energy injected into the ISM by the jet (Di Matteo et al. 2003), or by the presence of a binary black hole within the Bondi

radius, if the double optical nucleus (Laine et al. 2003) is interpreted this way. Another explanation to balance the energy output with requirements could be that the mass of the black hole is a factor 2 lower, and the density is similarly overestimated, which would reduce the energy output by 1 order of magnitude, commensurate with the kinetic energy estimated for the jet.

The black hole in the nucleus of M87 has a mass of $3 \times 10^9 M_{\odot}$ derived from HST spectroscopy (Ford et al. 1994; Harms et al. 1994; Macchetto et al. 1997). The Bondi accretion rate in M87 (Di Matteo et al. 2003) is $\sim 0.1 M_{\odot} \text{ y}^{-1}$, about eight times that in PKS 1246–410 predicting a nuclear luminosity of $5 \times 10^{44} \text{ erg s}^{-1}$. The kinetic energy estimated for the jets in M87 is at least $3 \times 10^{42} \text{ erg s}^{-1}$ (Owen et al. 2000; Young et al. 2002; Dunn & Fabian 2004), nearly an order of magnitude higher than estimated for PKS 1246–410. With a factor of ~ 10 for overpressured bubbles of relativistic particles, the output could be up to ten times larger. As for PKS 1246–410, this is still about 1 order of magnitude less than the predicted nuclear luminosity.

Another nearby cD elliptical galaxy that has been studied with Chandra is NGC 6166 (which hosts the radio source 3C 338) in A2199 (Di Matteo et al. 2001). In NGC 6166 the derived Bondi accretion rate is $0.03 M_{\odot} \text{ y}^{-1}$, providing a luminosity of $2 \times 10^{44} \text{ erg s}^{-1}$ and a similarly low X-ray luminosity and accretion efficiency is derived. The minimum kinetic energy estimated to inflate the observed bubbles is $5 \times 10^{55} \text{ erg}$ for the eastern bubble, and $17 \times 10^{55} \text{ erg}$ for the western bubble (Dunn & Fabian 2004). Again assuming growth at the buoyant velocity, the minimum kinetic energy estimate is $6 \times 10^{41} \text{ erg s}^{-1}$, but could be greater by a factor of 10 for overpressured bubbles of relativistic particles. The jets of NGC 6166 therefore require about a factor 30 less energy than available from Bondi accretion, somewhat less than for M87 and PKS 1246–410.

7. Conclusions

Along with M87 (Di Matteo et al. 2003), and NGC 6166 (Di Matteo et al. 2001), NGC 4696 provides a third elliptical galaxy where the accretion rate onto a supermassive black hole can be studied in detail. All three of these systems have inner bubbles traced by the thermal gas that allow for an estimation of the time-averaged kinetic energy of the jets (Dunn & Fabian 2004). These energies are systematically 10-30 times lower than the energy available from Bondi accretion (assuming 10% conversion efficiency). However, this narrow range of values and the equally remarkable narrow range in radiative efficiency for these systems, which are all low with $\eta = 1 - 2 \times 10^{-5}$, may indicate a universal property of accretion in the generation of jets, and will be explored further in a future paper (in preparation). A

low, but broader range of accretion efficiency of $\eta = 10^{-2}$ to 10^{-5} is found by Donato et al. (2004) for 13 FR I galaxies from the 3CR and B2 catalogs.

Di Matteo et al. (2003) suggest that M87 may be currently in a low state. With the addition of PKS 1246–410 to the small number of radio galaxies (including 3C338) for which the Bondi radius can be estimated, and an accurate value of the radiative efficiency calculated, this argument weakens. It is more likely that for the majority of the time the accretion efficiency is low.

We note that given its proximity and our estimated Lorentz factor of ~ 3 , the expected motion of the jet components in PKS 1246–410 is 2 mas yr^{-1} . This motion could be readily detected in VLBI observations spread out over a few months.

GBT acknowledges support for this work from the National Aeronautics and Space Administration through Chandra Award Numbers GO4-5134X and GO4-5135X issued by the Chandra X-ray Observatory Center, which is operated by the Smithsonian Astrophysical Observatory for an on behalf of the National Aeronautics and Space Administration under contract NAS8-03060. SWA thanks the Royal Society for support. This research has made use of the NASA/IPAC Extragalactic Database (NED) which is operated by the Jet Propulsion Laboratory, Caltech, under contract with NASA. The National Radio Astronomy Observatory is a facility of the National Science Foundation operated under a cooperative agreement by Associated Universities, Inc.

REFERENCES

- Aldcroft, T. L., Karovska, M., Cresitello-Dittmar, M. L., Cameron, R. A., & Markevitch, M. L. 2000, *Proc. SPIE*, 4012, 650
- Anders, E., & Grevesse, N. 1989, *Geochim. Cosmochim. Acta*, 53, 197
- Bernardi, M., Alonso, M. V., da Costa, L. N., Willmer, C. N. A., Wegner, G., Pellegrini, P. S., Rit e, C., & Maia, M. A. G. 2002, *AJ*, 123, 2159
- Cappellari, M., & Copin, Y. 2003, *MNRAS*, 342, 345
- Dickey, J. M., & Lockman, F. J. 1990, *ARA&A*, 28, 215
- Di Matteo, T., Quataert, E., Allen, S. W., Narayan, R., & Fabian, A. C. 2000, *MNRAS*, 311, 507
- Di Matteo, T., Johnstone, R. M., Allen, S. W., & Fabian, A. C. 2001, *ApJ*, 550, L19
- Di Matteo, T., Allen, S. W., Fabian, A. C., Wilson, A. S., & Young, A. J. 2003, *ApJ*, 582, 133
- Donato, D., Sambruna, R.M., & Gliozzi, M. 2004, *ApJ*, 617, 915
- Dunn, R. J. H., & Fabian, A. C. 2004, *MNRAS*, 355, 862
- Fabian, A. C., Sanders, J. S., Taylor, G. B., & Allen, S.W. 2005, *MNRAS*, in press
- Ford, H. C., et al. 1994, *ApJ*, 435, L27
- Fujita, Y., & Reiprich, T. H. 2004, *ApJ*, 612, 797
- Gebhardt, K., et al. 2000, *ApJ*, 543, L5
- Giovannini, G., Taylor, G. B., Feretti, L., Cotton, W. D., Lara, L., & Venturi, T. 2005, *ApJ*, 618, 635
- Harms, R. J., et al. 1994, *ApJ*, 435, L35
- Laine, S., van der Marel, R. P., Lauer, T. R., Postman, M., O’Dea, C. P., & Owen, F. N. 2003, *AJ*, 125, 478
- Macchetto, F., Marconi, A., Axon, D. J., Capetti, A., Sparks, W., & Crane, P. 1997, *ApJ*, 489, 579

- Owen, F. N., Eilek, J. A., & Kassim, N. E. 2000, *ApJ*, 543, 611
- Pinkney, J., et al. 2003, *ApJ*, 596, 903
- Reich, W., Fürst, E., Reich, P., Kothes, R., Brinkmann, W., & Siebert, J. 2000, *A&A*, 363, 141
- Sanders, J. S., & Fabian, A. C. 2002, *MNRAS*, 331, 273
- Taylor, G. B. 1996, *ApJ*, 470, 394
- Taylor, G. B., O’Dea, C. P., Peck, A. B., & Koekemoer, A. M. 1999, *ApJ*, 512, L27
- Taylor, G. B., Fabian, A. C., & Allen, S. W. 2002, *MNRAS*, 334, 769
- Salvati, M., Spada, M., & Pacini, F. 1998, *ApJ*, 495, L19
- Young, A. J., Wilson, A. S., & Mundell, C. G. 2002, *ApJ*, 579, 560

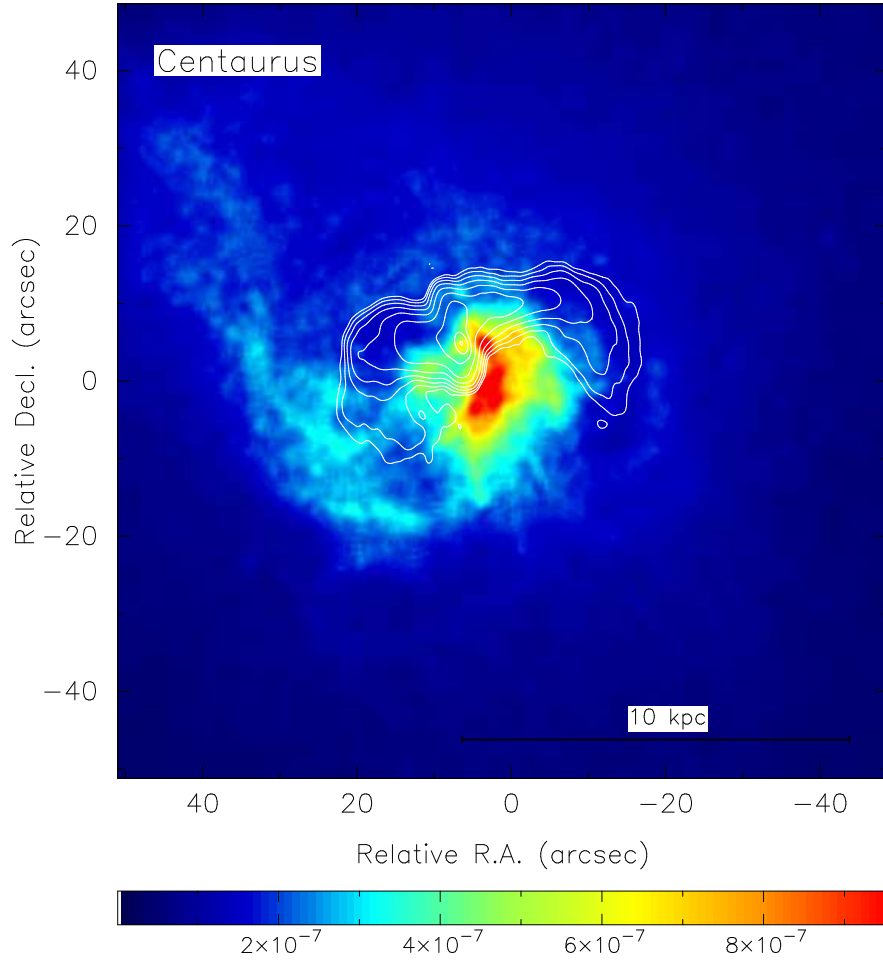


Fig. 1.— The central region of the Centaurus cluster in X-rays (color) and 5 GHz radio (contours). Contour levels begin at 0.4 mJy/beam and increase by factors of 2. The synthesised beam for the radio image is 2.1×1.2 arcseconds in position angle 19° . Coordinates are relative to the VLA pointing center at J2000 R.A. 12 48 48.7, Dec. $-41\ 18\ 44.0$.

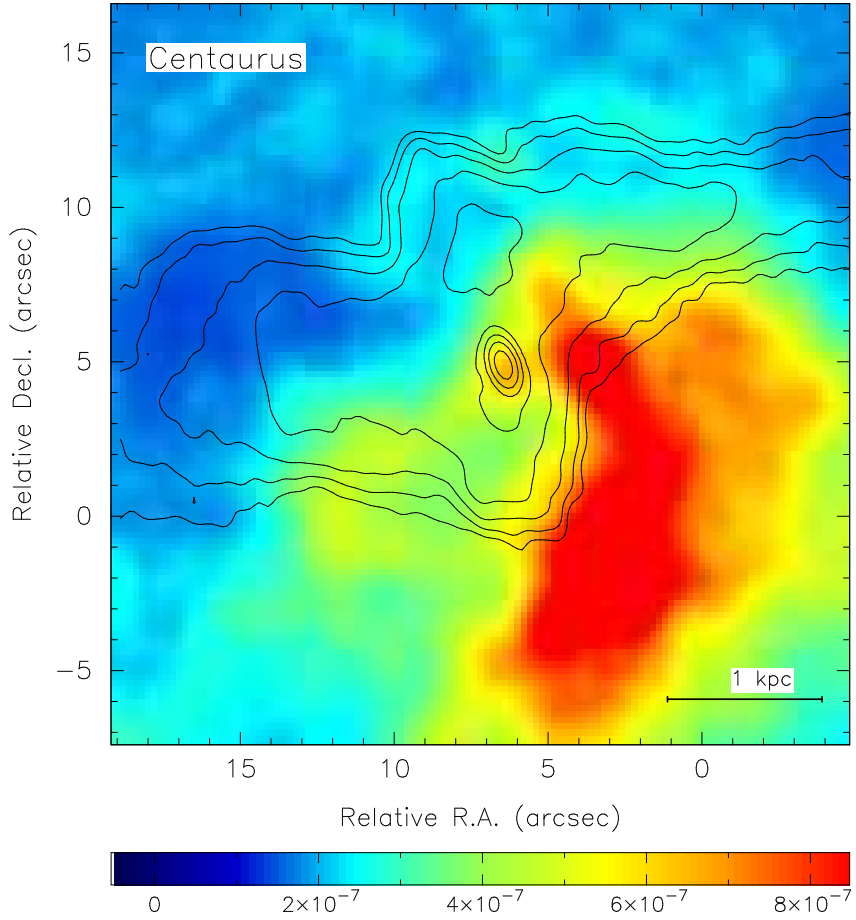


Fig. 2.— The central region of the Centaurus cluster in X-rays (color) and 8.4 GHz radio (contours). A weak X-ray point source is coincident with the bright radio core. The radio emission seems initially directed N-S, but clearly interacts with the thermal gas and ends up collimated E-W. Contour levels begin at 0.4 mJy/beam and increase by factors of 2. The synthesised beam for the radio image is 1.1×0.58 arcseconds in position angle 21° . The zero point for the coordinates is the same as in Fig. 1.

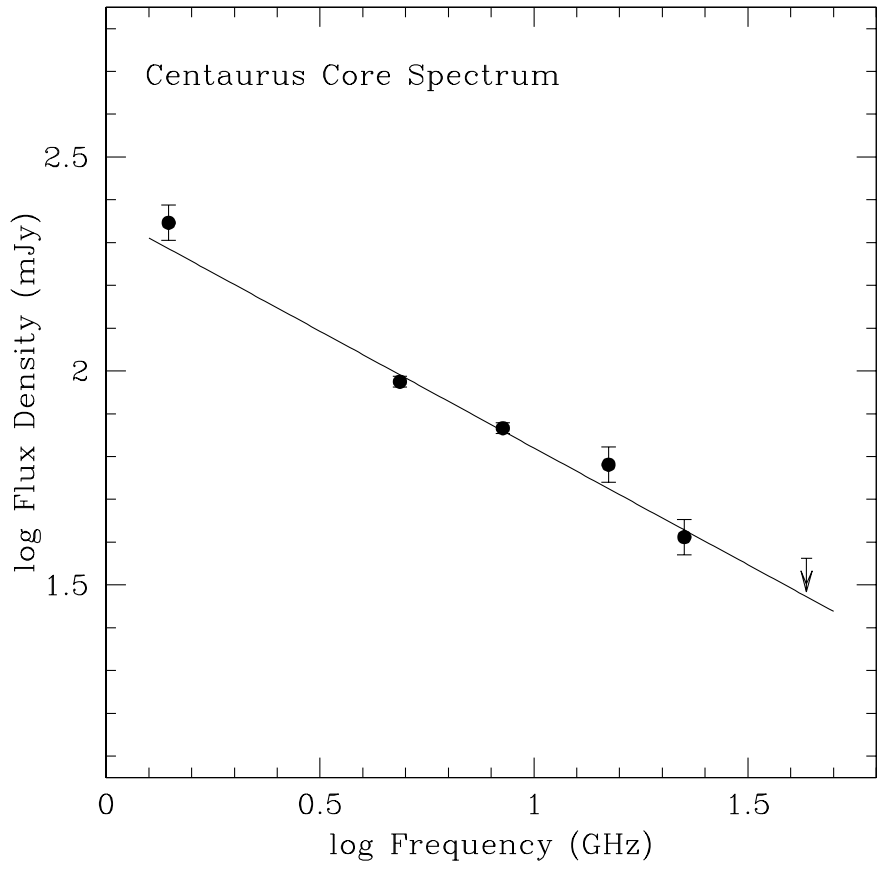


Fig. 3.— Spectrum of the nucleus of PKS 1246–410. The solid line is a least squares fit with slope -0.55 ± 0.04 .

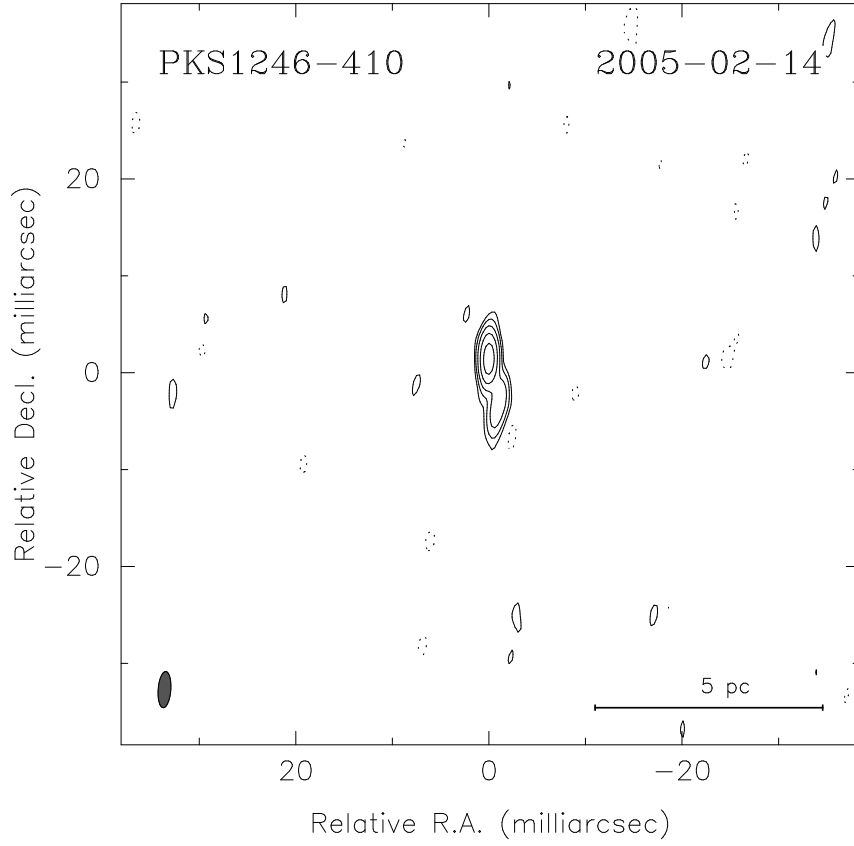


Fig. 4.— The full resolution image of PKS 1246–410 at 5.0 GHz. Contours start at 0.3 mJy/beam and increase by factors of 2. The restoring beam of 3.74×1.31 mas in position angle -4.3° is drawn in the lower left corner. Coordinates are relative to the nucleus at J2000 R.A. 12 48 49.2609, Dec. -41 18 39.417.

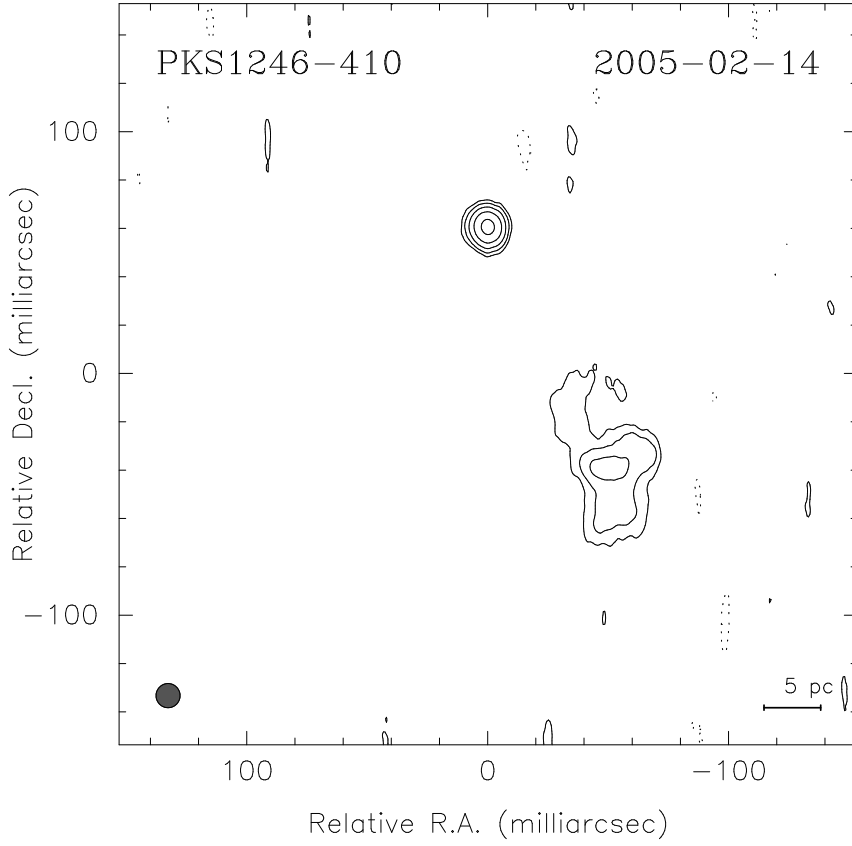


Fig. 5.— A tapered, low resolution image of PKS 1246-410 at 5.0 GHz. Contours start at 0.5 mJy/beam and increase by factors of 2. The restoring beam of 10 mas is drawn in the lower left corner. The zero point for the coordinates has been arbitrarily offset from the nucleus by 60 mas.

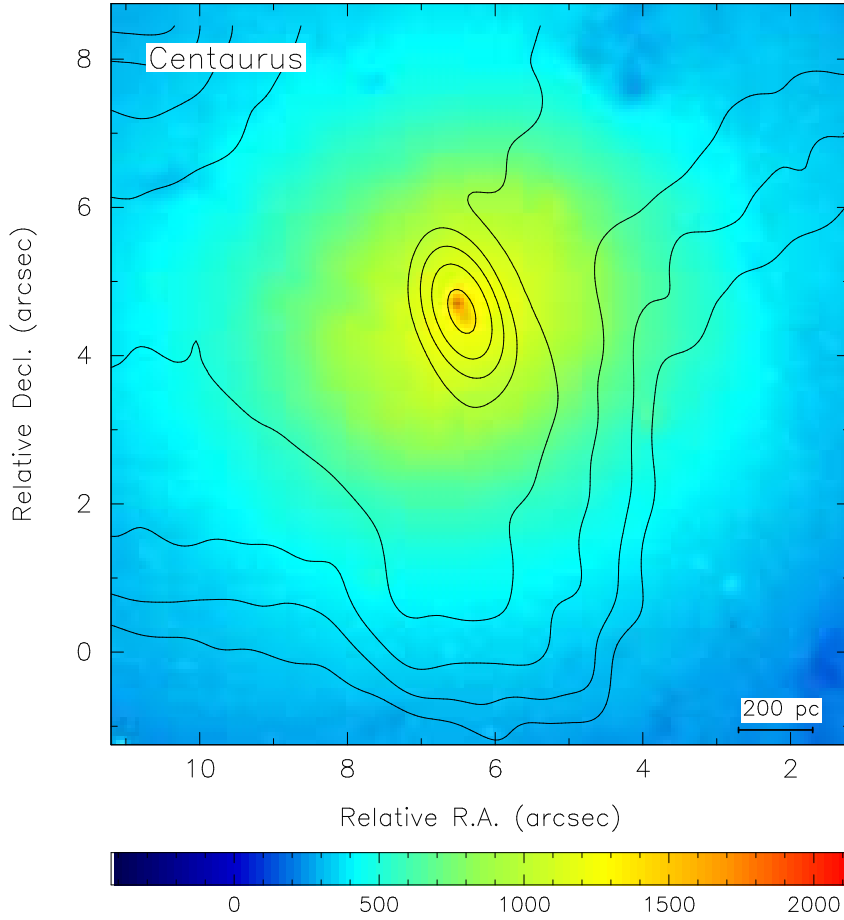


Fig. 6.— The central region of the Centaurus cluster from the HST at 7904 angstroms (color) and 8.4 GHz radio (contours). The HST image has been shifted by 0.4 arcsecond due north in order to align the centroid of the double optical nucleus with the radio core. The elongation of the radio core in the same position angle as the double optical nucleus is primarily the result of the synthesised beam which has dimensions 1.1×0.58 arcseconds in position angle 21° . Contour levels begin at 0.4 mJy/beam and increase by factors of 2. Coordinates are the same as Figures 1 and 2.

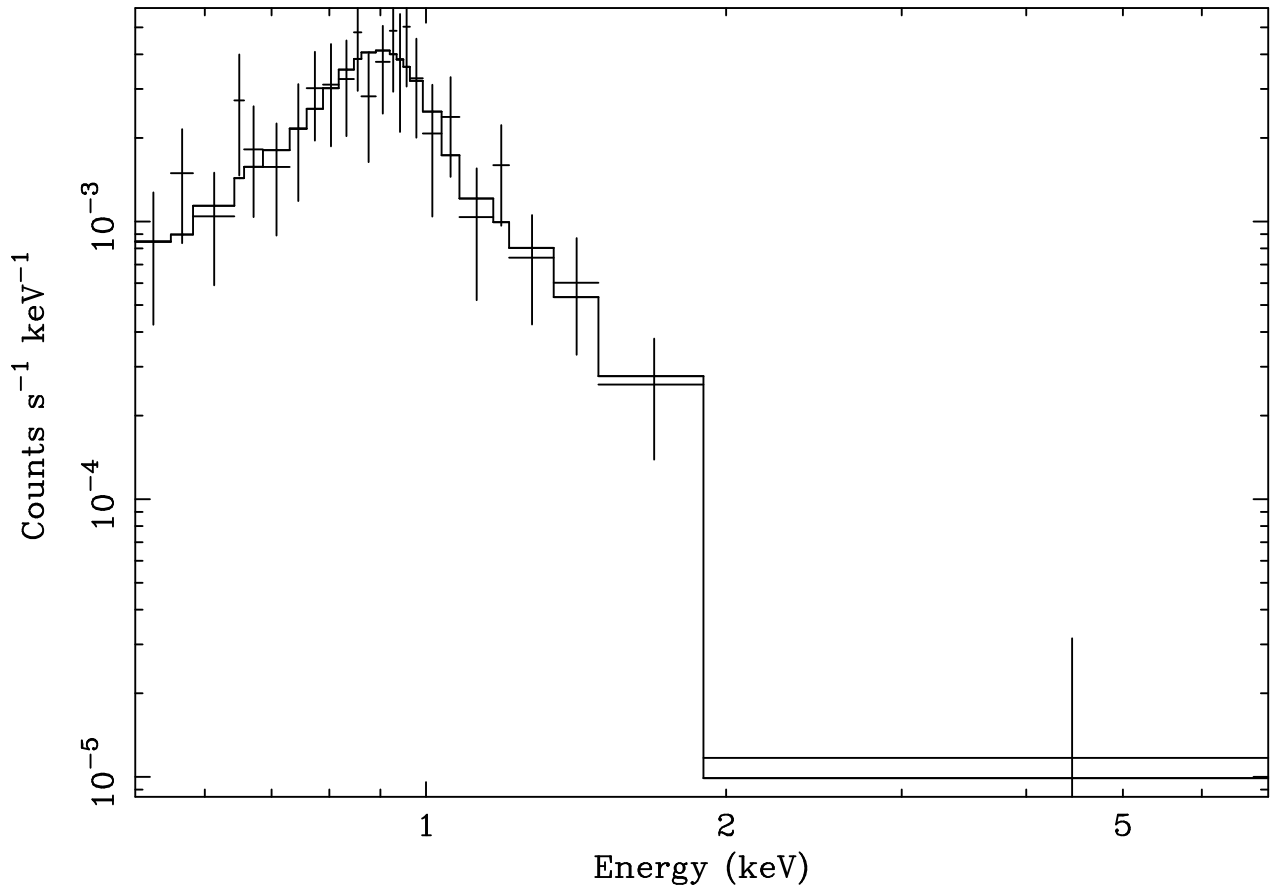


Fig. 7.— The X-ray spectrum at the nucleus fit with a mekal spectrum, with the absorption from the Dickey & Lockman results (plus an additional free absorption component at the redshift of the cluster). A region to the east of the nucleus, 1.1 to 2.7 arcsecs in radius, spanning 209° was used to calculate the background level.

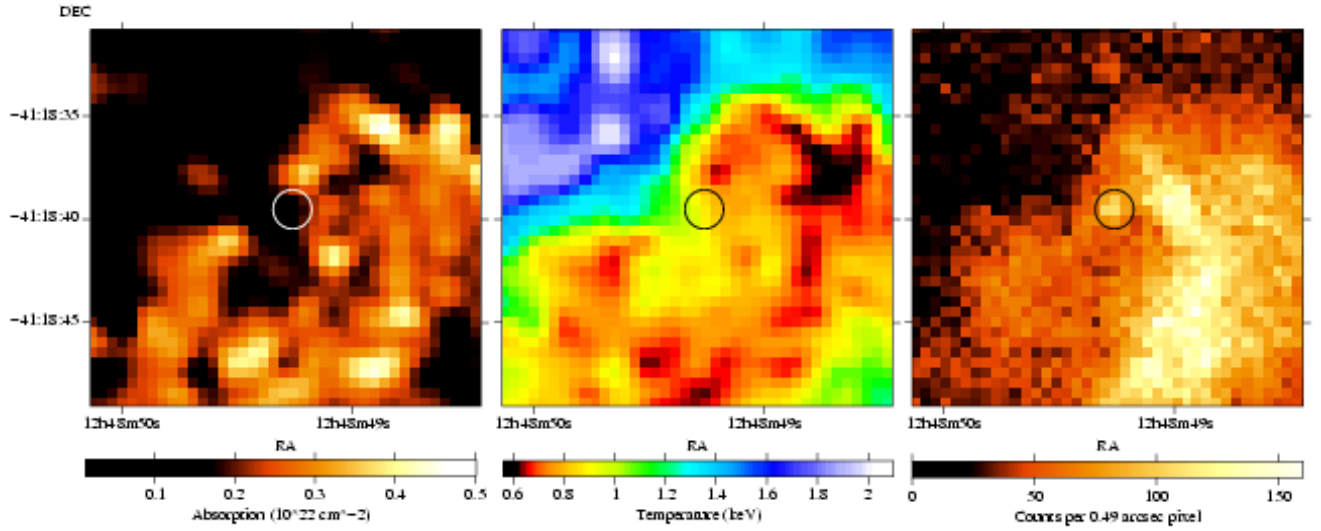


Fig. 8.— The derived temperature and absorption from fits to the Chandra X-ray observations of the inner part of the Centaurus cluster. The circle indicates the location of the nucleus.

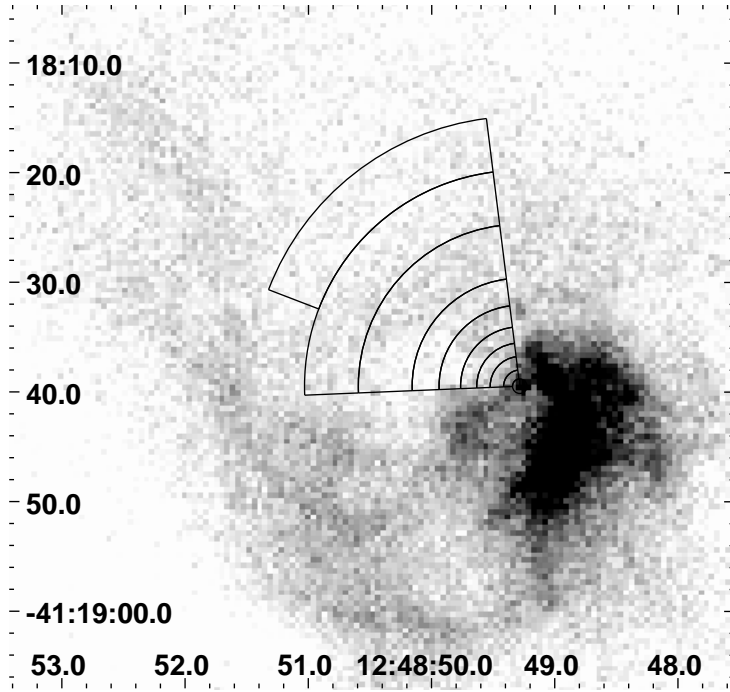


Fig. 9.— An unsmoothed X-ray image between 0.4 and 7 keV. The circular region used to extract the X-ray emission from the compact central component is overlaid, along with the incomplete annuli used to calculate the undisturbed radial profile.

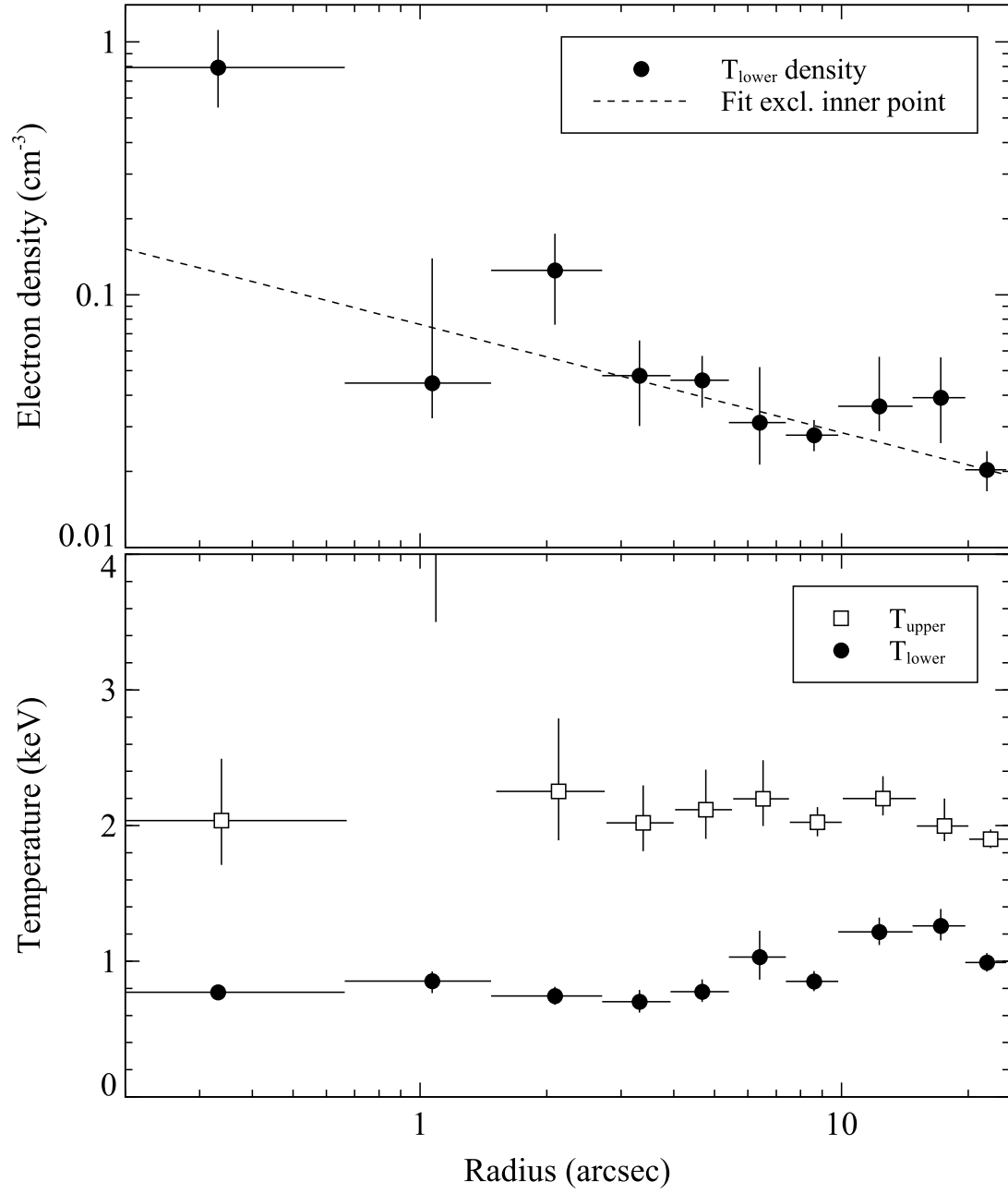


Fig. 10.— A fit to the temperature and density of the thermal gas in the central four kiloparsecs of the Centaurus cluster.

TABLE 1
RADIO OBSERVATIONAL PARAMETERS

Source	Date	Frequency (MHz)	Bandwidth (MHz)	Config.	Duration (min)
PKS 1246–410	Oct 2004	323/328	6.25	A	178
	Oct 2004	1365/1435	50	A	1
	Apr 1998	4635/4885	50	A	5
	Jun 1998	4635/4885	50	BnA	60
	Oct 2004	4885/4835	50	A	1
	Feb 2005	4986	32	VLBA	66
	Jun 1998	8115/8485	50	BnA	54
	Nov 1998	8115/8485	50	CnB	37
	Oct 2004	8435/8485	50	A	1
	Oct 2004	14965/14915	50	A	1
	Oct 2004	22485/22435	50	A	2
	Oct 2004	43315/43365	50	A	3

TABLE 2
VLA CORE FLUX DENSITY

Frequency (MHz)	Flux (mJy)	rms (mJy/beam)
1400	222 ± 22	0.56
4860	94.4 ± 2.8	1.3
8460	73.5 ± 2.2	0.50
14940	60.4 ± 6.0	0.73
22460	40.9 ± 4.1	0.59
43340	<36.5	3.3

TABLE 3
SOURCE PROPERTIES

Property	PKS 2322–123
core RA (J2000)	$12^h 48^m 49^s.2609$
Dec. (J2000)	$-41^\circ 18' 39''.417$
Gal. lat. (b)	21.56°
Gal. long. (l)	302.40°
radial velocity	$2958 \pm 15 \text{ km s}^{-1}$
distance from cluster center	0.0 Mpc
luminosity distance	43.0 Mpc
core flux density (5 GHz)	$9.0 \pm 0.5 \text{ mJy}$
core power (5 GHz)	$2.0 \times 10^{21} \text{ W Hz}^{-1}$
largest angular size	$150''$
largest physical size	30 kpc
total flux density (5 GHz)	1330 mJy
total power (5 GHz)	$3.0 \times 10^{23} \text{ W Hz}^{-1}$

TABLE 4
CHANDRA EXPOSURES

OBSID	Date	Clean exposure (ksec)	RA (J2000)	DEC (J2000)	Y offset (arcmin)
(1)	(2)	(3)	(4)	(5)	(6)
504	2000-05-22	21.8	12 48 48.7	-41 18 44.0	-1.0
505	2000-06-08	10.0	12 48 48.7	-41 18 44.0	-1.0
4954	2004-04-01	80.2	12 48 48.9	-41 18 44.4	-1.3
4955	2004-04-02	40.6	12 48 48.9	-41 18 44.4	-0.8
5310	2004-04-04	44.1	12 48 48.9	-41 18 44.4	-1.8

Notes: (1) Chandra Observation ID; (2) date of observation; (3) cleaned exposure time; (4) target RA and (5) DEC; (6) offset of the target from the aimpoint in the Y direction of the CCD.